International Journal of Mechanical, Industrial and Aerospace Sciences
ISSN: 2517-9950
Vol:6, No:8, 2012

A Comparison of Inflow Generation Methods for Large-Eddy Simulation

Francois T. Pronk, Steven J. Hulshoff.

Abstract—A study of various turbulent inflow generation methods was performed to compare their relative effectiveness for LES computations of turbulent boundary layers. This study confirmed the quality of the turbulent information produced by the family of recycling and rescaling methods which take information from within the computational domain. Furthermore, more general inflow methods also proved applicable to such simulations, with a precursor-like inflow and a random inflow augmented with forcing planes showing promising results.

Keywords—Boundary layer, Flat plate, Inflow modeling, LES

I. Introduction

PRACTICAL numerical simulation of realistic flows often requires that artificial boundaries be imposed between a flow region of interest and the part of the flow which one would like to avoid computing. The application of such artificial boundary conditions should ideally be done without influencing the solution within the computational domain. Spatially evolving turbulence poses an extra challenge when applying artificial boundary conditions, as in most cases the flow downstream is highly dependent on the conditions at the inflow. Ensuring the correct development of all turbulent properties therefore imposes stringent requirements on the inflow condition. Conversely, poorly-defined inflow conditions will result in undesirably long adaptation lengths, wasting useful computational resources. In this light, the following paper will provide an objective comparison of the performance of various turbulent inflow generation methods applied to the Large-Eddy Simulation (LES) of incompressible turbulent flat-plate boundary layers. The goal of this study is to determine which methods could be applicable to simulations of flow-control devices, where shape factor, boundary layer growth and skin friction are primary parameters of concern.

Early approaches to turbulent inflow modeling used random velocity fluctuations imposed on a mean flow. Although it is quite feasible to match the different moments and the energy spectra per wavelength using stochastic models, the phase information is somewhat more delicate to obtain, as it is strongly dependent on the type of flow and the location within the flow under consideration. Consequently the use of random velocity fluctuations had varying degrees of success. Using a fluctuation field based on a superimposition of Fourier modes with random-based phase, amplitude and anisotropy information, Batten *et al.* [1] reported that at least 20 inflow boundary layer thicknesses δ_0 were needed to obtain a physically realistic flow. Similarly, Lee *et al.* [2] reported needing over $12\,\delta_0$ for flow adjustment using velocity perturbations with a prescribed power spectrum and random phase information. More successfully, Pamiès *et al.* [3] improved on an approach by Marusic [4] who showed that channel flow mean and Reynolds stress profiles could be matched accurately by superimposing analytical hairpin-like vortical structures on a mean profile. They achieved realistic friction coefficient and shape factor growth within $6\,\delta_0$ of the inflow.

Another approach to the generation of inflow conditions for turbulent numerical simulations makes use of secondary simulations or precursor databases to provide turbulent information to a primary computation. This is often done using a separate calculation of an equilibrium flow with periodic boundary conditions, storing the velocity field of a plane normal to the streamwise direction at each time step, and then re-using the information obtained as inflow data for the simulation of more complex turbulent flows. A variant of such an approach was developed by Schlüter *et al.* [5] for hybrid RANS/LES computations, and showed good agreement with experimental results. The method had the advantage of not requiring the precursor simulation to be at the same Reynolds number as the LES study, or in the same configuration. An alternative approach was implemented by Druault *et al.* [6], who reconstructed data from experimental measurements to use as inflow condition for Large-Eddy Simulations. They claimed obtaining good results, although they did not specify the adaptation length required by their method.

A third type of inflow modeling strategy is based on the recycling type of inflows pioneered by Spalart and Leonard [7]. These methods rely on providing inflow conditions using turbulent information obtained from within a computational domain. A successful variant of this approach was developed by Lund *et al.* [8], and applied to flat plate computations. They extracted a velocity field downstream of the inflow, and rescaled it to compensate for boundary layer growth, achieving an adaptation length of $8\,\delta_0$. Simplifying the method by Lund *et al.*, Spalart *et al.* [9] further decreased the adaptation length to $4\,\delta_0$.

Although the Lund *et al.* family of inflows show very promising results, the rescaling procedures used are based on the assumption of equilibrium turbulent flows, limiting their scope of applicability. They have also been shown, in some cases, to add unphysical forcing to the computed flow due to the introduction of a form of temporal periodicity (see for instance Simens *et al.* [10]). Simulating more general wall-bounded turbulent flows will therefore require more versatile inflow conditions.

As explained in the first paragraph of this introduction, the goal of this paper is to make an objective comparison of

Faculty of Aerospace Engineering, Delft University of Technology.
Contact: s.j.hulshoff@tudelft.nl

recent inflow modeling techniques applicable to the simulation of turbulent wall-bounded flows, in the context of coarse Large-Eddy Simulations. The recycling and rescaling method of Lund *et al.* [8] was shown in previous publications to work well in LES, and will be chosen as reference inflow model. The simplified recycling inflow by Spalart *et al.* [9], originally applied to DNS, will also be tested. Furthermore, it will also be investigated whether more general inflow conditions could deliver performance comparable to that of recycling methods. To this end, a precursor-like method using rescaled channel-flow data will be tested, and a flow correction method developed by Spille-Kohoff and Kaltenbach [11] will be applied to a random inflow method, to assess whether it is accurate enough to remedy to the long adaptation lengths normally associated with random inflow conditions.

The remainder of this paper will be subdivided into 4 parts. First the various inflow generation methods will be presented briefly, then the comparison procedure and numerical setup will be introduced, followed by an analysis of the performance of the various inflows, and finally, the results will be summarized in a short conclusion.

II. Generation of Turbulent Inflow Data for Spatially Developing Boundary Layers

A. The Recycling Method by Lund, Wu and Squires [8]

The main idea behind the recycling and rescaling inflow modeling approach is to extract data at a station downstream from the inflow, and rescale it to account for boundary layer growth. In the approach by Lund *et al.*, the flow at the extraction station is averaged in spanwise direction and in time, to allow the decomposition of the flow field in a mean and a fluctuating part as

$$u_i'(x,y,z,t) = u_i(x,y,z,t) - U_i(x,y), \tag{1}$$

with x, y and z denoting the streamwise, wall-normal, and spanwise direction respectively. The mean velocities and fluctuations are then rescaled according to the law of the wall in the inner region and the defect law in the outer region, and blended together using a weighted average of the inner and outer profiles. The perturbations are rescaled according to

$$(u_i')_{\text{in}}^{\text{inner}} = \gamma\,(u_i')_{\text{recy}}(y_{\text{in}}^+, z, t) \tag{2}$$

and

$$(u_i')_{\text{in}}^{\text{outer}} = \gamma\,(u_i')_{\text{recy}}(\eta_{\text{in}}, z, t), \tag{3}$$

with the subscript $()_{\text{recy}}$ referring to the data from the recycling plane, the subscript $()_{\text{in}}$ to that from the inflow, and where the parameter γ is defined as $\gamma = u_{\tau,\text{in}}/u_{\tau,\text{recy}}$. The parameter η corresponds to outer-coordinates, defined as $\eta = y/\delta$, and y^+ corresponds to wall-units defined as $y^+ = yu_\tau/\nu$.

The rescaling of the mean profiles differs per flow component. The mean in x direction is rescaled as

$$U_{1,\text{in}}^{\text{inner}} = \gamma\, U_{1,\text{recy}}(y_{\text{in}}^+) \tag{4}$$

and

$$U_{1,\text{in}}^{\text{outer}} = \gamma\, U_{1,\text{recy}}(\eta_{\text{in}}) + (1-\gamma)U_\infty, \tag{5}$$

with U_∞ the freestream velocity. The mean velocity profile in y direction is rescaled as

$$U_{2,\text{in}}^{\text{inner}} = U_{2,\text{recy}}(y_{\text{in}}^+) \tag{6}$$

and

$$U_{2,\text{in}}^{\text{outer}} = U_{2,\text{recy}}(\eta_{\text{in}}). \tag{7}$$

The mean in z direction is set to zero as flows without spanwise gradients are considered here. The velocity profiles are then assembled as

$$\begin{aligned}(u_i)_{\text{in}} = &\left[(U_i)_{\text{in}}^{\text{inner}} + (u_i')_{\text{in}}^{\text{inner}}\right][1 - W(\eta_{\text{in}})] \\ &+ \left[(U_i)_{\text{in}}^{\text{outer}} + (u_i')_{\text{in}}^{\text{outer}}\right] W(\eta_{\text{in}}),\end{aligned} \tag{8}$$

with the weighting function $W(\eta)$ defined as

$$W(\eta) = \frac{1}{2}\left\{1 + \frac{1}{\tanh(\alpha)}\tanh\left[\frac{\alpha(\eta - b)}{(1-2b)\eta + b}\right]\right\}, \tag{9}$$

and the coefficients chosen as $\alpha = 4$ and $b = 0.2$.

Were interpolation is needed, Lund *et al.* found a linear interpolation to be sufficiently accurate for use with their second-order scheme.

B. Outer-Coordinate Rescaling

An outer-coordinate rescaling method similar to that by Spalart *et al.* [9] was also implemented as a simplification to the method by Lund *et al.* [8]. In this method the inflow velocity field is simply obtained by rescaling the velocity vector at the recycling station such that

$$U_{\text{in}}\left(0, \frac{y}{\delta_{\text{in}}}, z, t\right) = U_{\text{recy}}\left(x_{\text{recy}}, \frac{y}{\delta_{\text{recy}}}, z, t\right), \tag{10}$$

where δ corresponds to the 99%-thickness of the boundary layer.

Contrary to the original implementation by Spalart *et al.*, no shift in z coordinate was used. This choice is justified by the fact that in the simulations under consideration, the recycling planes are located at $400\,\theta_0$ from the inflow, which is beyond the eddy coherence length determined by Simens *et al.* [10] for this type of inflow.

C. Precursor Method

The precursor method implemented for the current study used data obtained from a secondary channel flow simulation, which was recycled and rescaled according to the method by Lund *et al.*, to provide as inflow condition. The channel flow was driven by a constant pressure gradient $\frac{d\overline{p}}{dx} = 1$. No special rescaling was developed to account for the non-zero Reynolds stresses in the middle of the channel flow, and it is anticipated that this will affect the adaptation length of the boundary layer.

D. Random Inflow Method, with Forcing by Spille-Kohoff and Kaltenbach [11]

A random turbulent inflow augmented with a forcing method by Spille-Kohoff and Kaltenbach was also implemented, to determine whether it could compete with recycled inflow methods. The search for a more general type of inflow method disqualified the use of elaborate random inflows calibrated for specific flow conditions, as in most practical problems, very little information is available *a priori* on the turbulent state within a computational domain. The inflow model chosen, although relatively simple, is a good example of what can be used in the context of mixed RANS/LES simulation, where the inflow has to be defined using the limited information available from a RANS solver.

The implementation of the current random inflow was inspired from that by Batten *et al.* [1], and is based on the construction of a perturbation field using Fourier modes with random phases and amplitudes, and scaled with a tensor scaling based on a Cholesky decomposition of the Reynolds stress tensor. The fluctuation field was computed using

$$v_j(z,t) = \sqrt{\frac{2}{N}} \sum_{n=1}^{N} p_j^n \cos\left(2\pi\varphi_j^n z + 2\pi\omega_j^n t + \phi_j^n\right), \quad (11)$$

where φ is the spatial phase, ω the temporal phase, and ϕ a random phase shift.

As LES is considered, special care should be taken to avoid unwanted physical forcing by adding modes at the inflow beyond what the mesh can represent. A sharp cut-off filter was implemented by choosing the random spatial phases such that the shortest wavelength imposed at the inflow spanned at least 10 cells. The range of the random temporal phase was determined using a Fast Fourier Transform of flat plate data obtained using the method by Lund *et al.* All variables were computed using random variables uniformly distributed between $[0,1]$ and then multiplied by the prescribed range. A random gaussian distribution could also be used instead. The inflow velocity field was then assembled with

$$u_i(y,z,t) = U_i(y) + \sum_j a_{ij} v_j(z,t), \quad (12)$$

where the amplitude tensor a_{ij} was related to the Reynolds stress tensor through

$$\begin{aligned} a_{11} &= \sqrt{R_{11}}, \\ a_{21} &= R_{21}/a_{11}, \\ a_{22} &= \sqrt{R_{22} - a_{21}^2}, \\ a_{33} &= \sqrt{R_{33}}, \end{aligned} \quad (13)$$

and were all a_{ij} elements not listed above were set to zero. For the current study, values for the Reynolds stress were obtained from DNS data.

To decrease the adaptation length of the random inflow, a forcing method by Spille-Kohoff and Kaltenbach [11] was used. This method compares a time-averaged Reynolds shear stress $<u'v'>$ at a location x_0 to a target Reynolds shear stress, and applies a forcing term to the wall-normal momentum equation to amplify or damp velocity fluctuations in that direction. The forcing term was determined using

$$f(x_0,y,z,t) = r(y,t)\left[u(x_0,y,z,t) - \langle U\rangle^{z,t}(x_0,y)\right], \quad (14)$$

with the amplitude defined as

$$r(y,t) = \alpha e(y,t) + \beta \int_0^t e(y,t')\,dt'. \quad (15)$$

The error function $e(y,t)$ was computed using

$$e(y,t) = -\rho\langle u'v'\rangle^{z,t}(x_0,y,t) - g(x_0,y), \quad (16)$$

where the $\langle\rangle^{z,t}$ exponents denote an average in spanwise direction and in time, and where $g(x_0,y)$ is the target stress. To avoid unrealistically large shear stress events, the forcing term f was only applied if the following conditions were satisfied: $|u'| < 0.6\,U_\infty$, $|v'| < 0.4\,U_\infty$, $u'v' < 0$, and $|u'v'| > 0.0015\,U_\infty^2$.

III. Comparison Procedure and Numerical Setup

The performance of the methods described in the previous section was evaluated through a study of the adaptation length required by the different type of inflows when applied to LES computations of turbulent boundary layers. The canonical zero-pressure gradient turbulent flat plate flow was chosen as computational test case, and the highest quality low Reynolds-number Direct Numerical Simulation (DNS) data available to date, that by Schlatter and Örlü [12] and that by Simens *et al.* [10], was used as reference solution.

To determine the adaptation length of the various methods, the evolution of the shape factor $H = \delta^*/\theta$ and the skin friction $c_f = 2\left(u_\tau/U_\infty\right)^2$ as a function of Reynolds number Re_θ was considered. The shape factor H was chosen as parameter as it was shown in Chauhan *et al.* [13] to be a sensitive indicator of the quality of the boundary layer, and has the advantage of not depending on estimates of skin friction, which can be subject to significant numerical errors in the context of LES. The evolution of skin friction coefficient was also considered, as it allows the indirect monitoring of the local level of turbulent activity within the boundary layer. The adaptation length was then defined as the domain length needed before the shape factor and skin friction coefficients followed a streamwise evolution similar to that of DNS. The longest of the two lengths was chosen as adaptation length.

The LES computations were performed on a $60\,\delta_0 \times 4\,\delta_0 \times 8\,\delta_0$ domain using a second-order finite-volume method. The mean freestream velocity and the viscosity were chosen such that $Re_\theta = 620$ at the inflow for the chosen initial boundary layer thickness δ_0. This combination of domain size and flow parameters also ensured that the domain height was at least twice that of the maximum boundary layer thickness in the domain, while capturing at least 5 to 6 low-speed streaks in spanwise direction. The domain was also long enough to ensure that the two lower Reynolds numbers stations from Schlatter and Örlü, $Re_\theta = 670$ and $Re_\theta = 1000$, could be reached, without being too close to the outflow boundary.

The flat plate grid used was uniform in all directions, with a resolution of $320 \times 64 \times 64$ cells. Periodic boundary conditions were used in spanwise direction. Neumann boundary conditions were used at the outflow and on the top of the domain

for the velocity, and at the inflow and the outflow for pressure. A Dirichlet boundary condition was applied for the pressure on top of the domain.

The channel flow simulation for the precursor method was run with a 64^3 mesh on a $6 \times 2 \times 4$ domain, ensuring the grid resolution was identical to that of the flat plate, at similar physical flow conditions. Periodic boundary conditions were used in spanwise and streamwise direction.

For the recycling methods, the extraction plane was placed at $48\,\delta_0$ from the inflow, or $400\,\theta_0$, beyond the coherence length of the eddies determined by Simens *et al.* [10].

When running the forcing method by Spille-Kohoff and Kaltenbach [11], 4 forcing planes where used at locations x/δ_0 = 0.6, 1.3, 2.6 and 5.2. In the current study, an averaging time window of $T_{\text{avg}} = 2\delta/U_\infty$ was used, together with $\alpha = 75$ and $\beta = 0$.

During the simulations, velocity means and perturbations were sampled and time averaged at several planes in streamwise direction. The mean velocities were first sampled for 5 time units before starting the perturbation sampling, which were sampled for another 35 time units. This is equivalent to the 1400 inertial timescales δ_0/U_∞ used by Lund *et al.*

Due to under resolution in the viscous sublayer, skin friction coefficients computed using finite difference led to underpredictions by about 10%. This was also observed by Sagaut *et al.* [14] and Spyropoulos and Blaisdell [15]. To overcome this underprediction, new friction coefficients were determined using a Clauser chart technique, in which the streamwise mean velocity profile is fitted to the logarithmic law of the wall. This fit yields a viscous velocity u_τ, from which a new friction coefficient can be determined. This method is often used in experimental flat plate boundary layer measurements, although there is some debate on the exact values to be used for the law of the wall. More details on the Clauser chart technique can be found in Wei *et al.* [16]. Other methods based on velocity profile fitting have also been investigated, but proved cumbersome and less accurate. An exception was a U^+ as a function of Re_θ estimate, by Monkewitz *et al.* [17], from which an approximation for u_τ could be extracted, knowing U_∞. It returned results very similar to those obtained using the Clauser chart technique.

IV. Results

The streamwise mean flow and Reynolds stress averages obtained using the recycling method by Lund *et al.* are presented in fig. 1 and 2. The data corresponds to a sampling station were the local Reynolds number is $Re_\theta = 670$.

From figure 1, it can be seen that the streamwise mean velocity is well captured by the grid, even though the mesh resolution near the wall is relatively low. The matching of the profile with DNS data at $y/\delta > 1$ also illustrates that the Clauser chart technique used accurately estimates the local viscous velocity u_τ.

Considering the Reynolds stresses shown in Fig. 2, one can see that the $\overline{u'^2}^+$ and $\overline{w'^2}^+$ Reynolds stresses are slightly overpredicted, with a noticeable peak close to the wall. These peaks were attributed to under-resolution in the near-wall

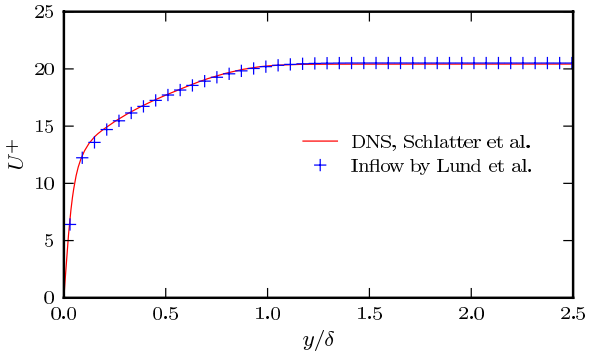

Fig. 1. Mean velocity as a function of y/δ. The line represents DNS data by Schlatter and Örlü [12]

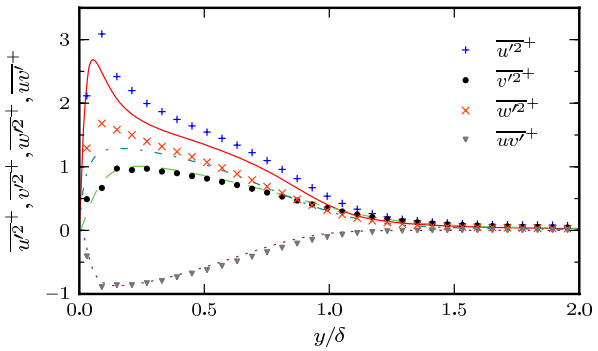

Fig. 2. Rms as a function of y/δ. The lines represent DNS data by Schlatter and Örlü [12].

region, and were shown to decrease when increasing the grid resolution. On the other hand, the $\overline{v'^2}^+$ and $\overline{uv'}^+$ stresses are well captured by the mesh, albeit it with, respectively, a slight underprediction and overprediction.

From there, the shape factor and skin friction coefficient evolution of the different inflow generation methods can be compared. Fig. 3 compares the evolution of the shape factor H as a function of Re_θ with DNS data and with an empirical shape factor fit based on experimental data, taken from Monkewitz *et al.* [17], and plotted with a $\pm 2\%$ tolerance. It is important to underline that this empirical formula was derived using medium to high Reynolds number experimental data, and therefore solely serves as a qualitative approximation of the shape factor evolution. Similarly, the evolution of the recomputed friction coefficients was compared to DNS data and to an empirical friction coefficient fit by Smits *et al.* [18]. This fit, based on a power law, estimates the friction coefficient as $c_f = 0.024\,\text{Re}_\theta^{-1/4}$ and was shown by Schlatter and Örlü [12] to be a surprisingly accurate fit to low Reynolds number DNS friction coefficients. It is plotted in Fig. 4 with a $\pm 5\%$ tolerance.

The benchmark recycling method of Lund *et al.* and that of Spalart *et al.* show very similar shape factor evolution in Fig. 3, although the Reynolds number at the first sampling

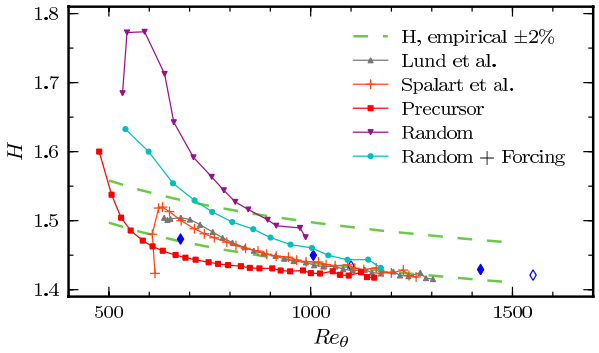

Fig. 3. Shape factor H, as a function of Re$_\theta$. ◆: DNS data points from Schlatter and Örlü [12], ◇: DNS data points from Simens *et al.* [10]

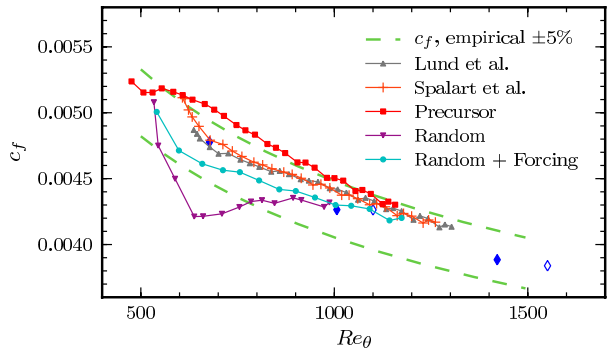

Fig. 4. Skin coefficient c_f, as a function of Re$_\theta$. ◆: DNS data points from Schlatter and Örlü [12], ◇: DNS data points from Simens *et al.* [10]

station of the method by Spalart *et al.* appears to be slightly lower than the expected value of $Re_\theta = 620$. Nonetheless, both methods show a reliable shape factor growth. Despite underpredicting the absolute shape factor when compared to the recycling method by Lund *et al.*, the precursor method seems to result in a shape factor following the correct growth trend. The effect of the forcing method by Spille-Kohoff and Kaltenbach on the random inflow is clear visible. Compared to the random inflow without forcing, the random inflow with forcing planes displays a much more realistic evolution of the shape factor. It is also clear that a simulation using the random inflow generation method alone would be unable to simulate a correct boundary layer growth within the current domain length used.

Similar trends can be observed in the evolution of the skin friction, as shown in Fig. 4. Once more, the recycling methods by Lund *et al.* and Spalart *et al.* produce very similar results, although it can be argued that recycling method by Spalart *et al.* needs a slightly longer adaptation length before following the same evolution trend as the method by Lund *et al.* The precursor method correctly simulates a decreasing skin friction with increasing Reynolds number, albeit with an overestimation of the skin-friction, and with a more or less linear decay. And finally, when considering the random inflows, the effects of the forcing planes are substantial, once again. Indeed, the random inflow with forcing planes has a more predictable and realistic skin friction coefficient evolution than the baseline random inflow. Moreover, it is interesting to notice that, after adaptation, the skin friction coefficient evolution of the random inflow with forcing planes is almost parallel to that of the recycling type of inflows.

A qualitative determination of adaptation lengths can be made for the various inflow methods using Fig. 3 and 4. Although the reference inflow model by Lund *et al.* and that from Spalart *et al.* show a very different shape factor evolution in the first 100 Re_θ of the computational domain, as shown in Fig. 3, they tend to follow a similar evolution trend after $Re_\theta = 860$, and, arguably, also follow the DNS trend from that point onwards. This corresponds to an adaptation length of $18\,\delta_0$ for the method by Lund *et al.* and a length of $22\,\delta_0$ for the method by Spalart *et al.* The shape factor evolution of the precursor method shows an evolution similar to DNS relatively rapidly, at around $Re_\theta = 700$. This corresponds to an adaptation length of $18\,\delta_0$, which is similar to that determined for the method by Lund *et al.* Unfortunately, with the current domain length, no true adaptation length can be determined from the shape factor evolution of the random inflow, as it does not noticeably follow the evolution of DNS at any part. Switching to the random inflow with forcing, it can be argued that its shape factor evolution follows DNS from $Re_\theta = 900$ onwards, corresponding to an adaptation length of $30\,\delta_0$.

In Fig. 4, the friction coefficient evolution of both recycling inflow methods display a much smoother and comparable evolution than the shape factor. A clear jump in skin friction can be observed at around $Re_\theta = 700$ for the method by Lund *et al.*, after which it arguably more or less follows the DNS evolution. This corresponds to an adaptation length of $6.5\,\delta_0$. The skin friction of the method by Spalart *et al.* also show a clear inflection point at $Re_\theta = 670$, after which it follows an evolution similar to the method by Lund *et al.*, corresponding to an adaptation length $8\,\delta_0$. Although the skin friction coefficient evolution of the precursor method does not seem to follow the slightly curved decay a correct evolution should have, its skin friction evolution seems to follow a smooth trend from $Re_\theta = 550$ onwards. This corresponds to an adaptation length of $8\,\delta_0$. And finally, as for the shape factor, it is once more difficult to determine an adaptation length of the random inflow, as it does not converge towards DNS evolution within the domain length used. The random inflow with forcing planes, on the contrary, rapidly converges towards a stable evolution, from $Re_\theta = 600$ onwards. This corresponds to an adaptation length of $8\,\delta_0$.

It interesting to notice that, contrary to the shape factor adaptation lengths, the skin friction adaptation lengths of the recycled type inflows are comparable to that determined by the authors of the original inflow methods.

Choosing the longest of the two adaptation lengths for every test case, it can be determined that the recycling and rescaling method by Lund *et al.* has the shortest adaptation length, on par with that from the precursor method, at $18\,\delta_0$, followed by the inflow generation method by Spalart *et al.* with an adaptation length of $22\,\delta_0$, and trailed by the random inflow

with forcing planes with an adaptation length of $30\,\delta_0$.

As a closing remark, it can be observed that Fig. 3 and 4 show oscillations in their value at higher Reynolds numbers, going downstream. This is caused by the influence of the numerical outflow, of Neumann type, which creates an abrupt truncation of the vortices leaving the domain. To try to remedy to this problem, both an advective and a convective type of outflow boundary conditions were tested, and proved effective in reducing the oscillations at the outflow, at the cost of creating oscillations at the inflow when recycling is used. The original Neumann outflow boundary condition was therefore kept.

V. Conclusions

Five inflow generation methods were applied to the simulation of incompressible flat plate boundary layers in the context of coarse Large-Eddy Simulations. The results confirm that both the recycling procedure by Lund *et al.* [8] and that by Spalart *et al.* [9] performed well in the context of equilibrium turbulent flows, showing the most consistent results, with adaptation lengths based on shape factor of $18\,\delta_0$ and $22\,\delta_0$ respectively. However, these long adaptation lengths arose from the slow convergence of the shape factor both methods displayed, going downstream. As the adaptation lengths determined from the skin friction coefficient evolutions were much shorter, this a confirmation that the shape factor is a more sensitive parameter to boundary layer quality than the skin friction.

However, this work was also oriented towards the testing of inflow generation methods which are independent of the flow conditions within the domain, as they could also be applied to the simulation of more demanding types of flows, where no equilibrium turbulence region exists. In this light, the precursor-like method showed a very promising adaptation length of $18\,\delta_0$, albeit with a slight underprediction of the shape factor and a small overprediction of the skin friction evolution.

Similarly, the random inflow method augmented with the forcing method by Spille-Kohoff and Kaltenbach [11] was also shown to be competitive, although this was poorly reflected by the long adaptation length of $30\,\delta_0$, which was due to a slow convergence of the shape factor evolution. In contrast, the skin friction adaptation was similar to that of the recycling methods, albeit slightly shifted downwards. It should be noted that the random inflow has the added advantage over the precursor method to be easily usable in coupling with a RANS solver, as it can use the Reynolds stress information from the RANS turbulence model as input for the inflow.

Finally, the random inflow without forcing planes was found to be uncompetitive, as its shape factor and skin friction evolution did not approach that of DNS within the current domain size tested.

References

[1] P. Batten, U. Goldberg, and S. Chakravarthy, "Interfacing Statistical Turbulence Closures With Large-Eddy Simulation: Boundary Conditions For Large-Eddy Simulation," *AIAA Journal*, vol. 42, no. 3, pp. 485–492, 2004.

[2] S. Lee, S. K. Lele, and P. Moin, "Simulation of spatially evolving turbulence and the applicability of Taylorś hypothesis in compressible flow," *Physics of Fluids A: Fluid Dynamics*, vol. 4, pp. 1521–1530, 1992.

[3] M. Pamiès, P. Weiss, E. Garnier, S. Deck, and P. Sagaut, "Generation of synthetic turbulent inflow data for large eddy simulation of spatially evolving wall-bounded flows," *Physics of Fluids*, vol. 21, p. 045103, 2009.

[4] I. Marusic, "On the role of large-scale structures in wall turbulence," *Physics of Fluids*, vol. 13, pp. 735–743, 2001.

[5] J. Schlüter, H. Pitsch, and P. Moin, "Large Eddy Simulation Inflow Conditions for Coupling with Reynolds-Averaged Flow Solvers," *AIAA journal*, vol. 42, no. 3, pp. 478–484, 2004.

[6] P. Druault, J. F. Largeau, F. Coiffet, J. Delville, J. P. Bonnet, and S. Lardeau, "Numerical Investigations of Turbulent Inflow Condition Generation for LES," *Journal of Fluids Engineering*, vol. 127, no. 5, pp. 945–948, 2005.

[7] P. R. Spalart and A. Leonard, "Direct numerical simulation of equilibrium turbulent boundary layers," in *IN: Symposium on Turbulent Shear Flows, 5th, Ithaca, NY, August 7-9, 1985, Proceedings (A86-30201 13-34). University Park, PA, Pennsylvania State University, 1985, p. 9.35-9.40.*, 1985.

[8] T. S. Lund, X. Wu, and K. D. Squires, "Generation of Turbulent Inflow Data for Spatially-Developing Boundary Layer Simulations," *Journal of Computational Physics*, vol. 140, no. 2, pp. 233–258, 1998.

[9] P. Spalart, M. Strelets, and A. Travin, "Direct numerical simulation of large-eddy-break-up devices in a boundary layer," *International Journal of Heat and Fluid Flow*, vol. 27, no. 5, pp. 902–910, 2006.

[10] M. P. Simens, J. Jiménez, S. Hoyas, and Y. Mizuno, "A high-resolution code for turbulent boundary layers," *Journal of Computational Physics*, vol. 228, no. 11, pp. 4218–4231, 2009.

[11] A. Spille-Kohoff and H.-J. Kaltenbach, "Generation of turbulent inflow data with a prescribed shear-stress profile," 2001.

[12] P. Schlatter and R. Örlü., "Assessment of direct numerical simulation data of turbulent boundary layers," *Journal of Fluid Mechanics*, vol. 659, no. 1, pp. 116–126, 2010.

[13] K. A. Chauhan, P. A. Monkewitz, and H. M. Nagib, "Criteria for assessing experiments in zero pressure gradient boundary layers," *Fluid Dynamics Research*, vol. 41, p. 021404, 2009.

[14] P. Sagaut, E. Garnier, E. Tromeur, L. Larchevêque, and E. Labourasse, "Turbulent Inflow Conditions for Large-Eddy Simulation of Compressible Wall-Bounded Flows," *AIAA Journal*, vol. 42, no. 3, pp. 469–477, 2004.

[15] E. T. Spyropoulos and G. A. Blaisdell, "Large-Eddy Simulation of a Spatially Evolving Supersonic Turbulent Boundary-Layer Flow," *AIAA journal*, vol. 36, no. 11, pp. 1983–1990, 1998.

[16] T. Wei, R. Schmidt, and P. McMurtry, "Comment on the Clauser chart method for determining the friction velocity," *Experiments in Fluids*, vol. 38, no. 5, pp. 695–699, 2005.

[17] P. A. Monkewitz, K. A. Chauhan, and H. M. Nagib, "Self-consistent high-reynolds-number asymptotics for zero-pressure-gradient turbulent boundary layers," *Physics of Fluids*, vol. 19, p. 115101, 2007.

[18] A. Smits, N. Matheson, and P. Joubert, "Low-reynolds-number turbulent boundary layers in zero and favorable pressure gradients," *Journal of ship research*, vol. 27, no. 3, pp. 147–157, 1983.